

Astronomy & Astrophysics manuscript no.
(will be inserted by hand later)

Continuous stellar mass-loss in N-body models of galaxies

Bruno Jungwiert¹, Françoise Combes² and Jan Palouš¹

¹ Astronomical Institute, Academy of Sciences of the Czech Republic, Boční II 1401, CZ-141 31 Prague 4
e-mail: bruno@ig.cas.cz

² DEMIRM, Observatoire de Paris, 61 Avenue de l'Observatoire, F-75 014 Paris

Received 22 May 2001; accepted 4 July 2001

Abstract. We present an N-body computer code – aimed at studies of galactic dynamics – with a CPU-efficient algorithm for a continuous (i.e. time-dependent) stellar mass-loss. First, we summarize available data on stellar mass-loss and derive the long-term (20 Gyr) dependence of mass-loss rate of a coeval stellar population. We then implement it, through a simple parametric form, into a particle-mesh code with stellar and gaseous particles. We perform several tests of the algorithm reliability and show an illustrative application: a 2D simulation of a disk galaxy, starting as purely stellar but evolving as two-component due to gradual mass-loss from initial stars and due to star formation. In a subsequent paper we will use the code to study what changes are induced in galactic disks by the continuous gas recycling compared to the instantaneous recycling approximation, especially the changes in star formation rate and radial inflow of matter.

Key words. stars: mass-loss – galaxies: evolution – galaxies: kinematics and dynamics – galaxies: spiral – methods: N-body simulations

1. Introduction

During the last decade, many N-body simulations (e.g. Friedli & Benz 1993; Junqueira & Combes 1996) as well as theoretical works on two-fluid gravitational instabilities (Jog 1992, 1996) have underlined the importance of the gas mass fraction for the dynamics and evolution of galaxies.

Gas crucially conditions star formation and evolution of large-scale instabilities (e.g. bars, spiral arms). In turn, star formation and large-scale flows induced by these instabilities influence mass and chemical profiles of galaxies (e.g. Martinet & Friedli 1997; Portinari & Chiosi 2000).

The gas content in a given area is determined by the competing processes of star formation and stellar mass-loss and by spatial flows of gas. A coherent picture of galactic evolution must therefore consistently couple stellar and gaseous dynamics with star formation and stellar evolution.

Star formation is, in large-scale models of galaxies, typically implemented through simplistic parametrizations reflecting mainly the energy supply from young stars and the gas mass fraction locked in newly born stars. On the other hand, stellar mass-loss has received much less attention from galactic N-body modellers since it was for a long time considered as a secondary issue. But nowadays, both observations and stellar evolutionary models (see Sect. 2

for references) indicate that the gas mass fraction restituted by stars is huge and may reach, when integrated over the stellar mass spectrum, some 45% over the Hubble time. Stars thus represent not only a place for permanent gas blocking but also an important temporary reservoir of gas that will be gradually reinjected into the interstellar medium.

Recent computer models of galactic dynamics usually approximate the stellar mass-loss as instantaneous, i.e. happening at the moment of stellar birth. Nonetheless, stars lose matter during all their lives. Stellar lifetimes span a very large range and in the case of low-mass stars they compare with or overpass the Hubble time. The use of the instantaneous recycling approximation, which was proposed by Tinsley (1980) for high mass-stars, is therefore not satisfactory for the whole stellar mass spectrum.

From the above emerges an obvious motivation for building a computer code able to follow the galactic structure and dynamics together with a non-instantaneous gas recycling. One can expect that the connection of such a recycling with the dynamics will affect large-scale gravitational instabilities, spatial flows of matter, star formation and gas consumption rates, etc., and thus the long-term evolution of galaxies.

The development and presentation of such a code is the central aim of this paper. Our model is innovative especially in introducing a continuous (i.e. time-dependent) gas recycling scheme, grafted on an underlying N-body

code using standard techniques for computing gravitational field (particle-mesh method) and gas dynamics (sticky-particles).

The text is organized as follows. In Sect. 2, we describe data and steps in deriving the time-dependence of mass-loss of a computer stellar particle. This curve, simply parametrized, is the key input information for our N-body code, however it can be useful also for other models (not necessarily N-body) of galaxies or star clusters. Section 3 presents our computer code, the emphasis being put on the implementation of the mass-loss. An instructive simulation of a barred galaxy is shown in Sect. 4. Section 5 summarizes the outcome and future prospects.

2. Stellar mass-loss and long-term galactic evolution

2.1. Mass-loss rate of a coeval stellar population

Stars of all masses lose matter via stellar winds, high-mass stars, in addition, in supernova explosions. Despite the fact that stellar winds accompany all stages of stellar evolution (see de Jager et al. 1988, for observations of wind rates across the Hertzsprung-Russell diagram), they vary in intensity and duration: gas is not released uniformly over a stellar lifetime but typically in a few relatively short episodes.

The time dependence of mass-loss rate of a coeval stellar population (hereafter CSP), $\dot{M}(t)$, could in principle be obtained if we knew the stellar initial mass function (IMF), $\psi(m_i)$, and the time dependence of the mass-loss rate of individual stars, \dot{m} :

$$\dot{M}(t) = \int_{m_{\min}}^{m_{\max}} \dot{m}(t, m_i) \psi(m_i) dm_i \quad (1)$$

Since neither the former nor the latter are known with much precision, we shall limit ourselves to construct a model curve based on several simplifying assumptions adequate to the purpose of the work which is to simulate the effects of stellar mass-loss on the *long-term* evolution of galaxies; we do not pretend to model changes occurring on a time-scale of less than ~ 10 Myr that is short compared to the dynamical time at most galactocentric distances.

Mass-loss for stars of different masses and evolutionary stages is reviewed in more detail in Jungwiert (1998) where references can be found for both observations and models. Here, only a brief summary of the most important mass-loss mechanisms is given: a) in the case of low-mass stars (LMS, hereafter defined as stars with initial masses $m_i < 2 M_{\odot}$), winds on the red giant branch (RGB) and asymptotic giant branch (AGB) are the most efficient; b) for intermediate-mass stars (IMS, $2 M_{\odot} < m_i < 8 M_{\odot}$), the AGB winds dominate; c) in the case of high-mass stars (HMS, $m_i > 8 M_{\odot}$), supernova explosions, Wolf-Rayet winds and main-sequence winds, contribute to the overall mass-loss in proportions strongly depending on m_i ; mass-loss is dominated by supernovae for $m_i < 25 M_{\odot}$, while

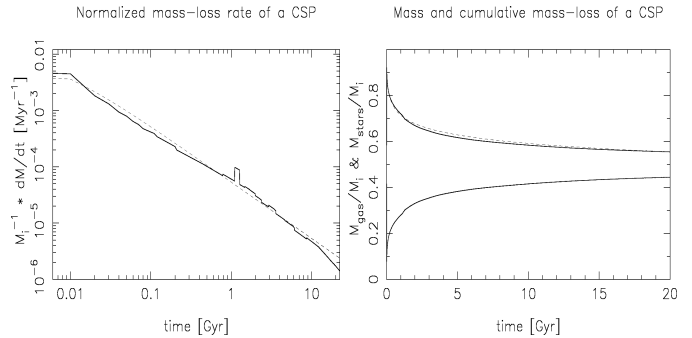


Fig. 1. **Left:** Normalized mass-loss rate, $\dot{M}(t)/M_i$, of a coeval stellar population (CSP) with $Z = 0.02$ and the Scalo's (1998) IMF. The full curve is derived from the Padua stellar models, the dashed curve is the fit corresponding to Eq. (2) with parameters from Table 1 (for $\tau = 20$ Gyr). Note that both scales are logarithmic. **Right:** Normalized stellar mass, M_{stars}/M_i (upper full curve), and the cumulative mass-loss (i.e. the released gas mass), M_{gas}/M_i (lower full curve), for the same CSP. The dashed curve corresponds to the normalized stellar mass computed for the mass-loss rate fit from the left panel.

for more massive stars the winds are more efficient than supernovae.

With regard to the above, we shall assume, for simplicity, that: a) for LMS all the mass-loss takes place in two distinct delta function events corresponding to the tips of RGB and AGB (since the respective winds strongly peak near these tips); b) for IMS and HMS, we treat the mass-loss as one delta function at the end of their lives: this reflects the AGB wind peak for intermediate-mass stars and SN explosion + winds for high-mass stars (as the most massive HMS, for which the winds dominate over supernovae, have very short lifetimes – less than 5 Myr for $m_i > 40 M_{\odot}$ – the delta function representation is adequate).

Necessary ingredients to construct an approximate mass-loss curve of a CSP thus reduce to the knowledge of IMF, stellar initial-final mass relation and stellar lifetime-mass relation (in the case of LMS, two lifetimes are necessary, for the ends of the RGB and AGB phases). As for the IMF, we use the power-law with three slopes (0.2, 1.7 and 1.3 for initial mass ranges of $0.1-1 M_{\odot}$, $1-10 M_{\odot}$ and $10-100 M_{\odot}$, respectively) inferred by Scalo (1998) as the “average” of recently published IMFs. For the initial-final mass relation and lifetime-mass relation, we rely on the Padua stellar evolutionary models (Bressan et al. 1993; Marigo et al. 1996) computed for the initial metallicity $Z = 0.02$.

The mass-loss rate function, $\dot{M}_n(t)$, constructed in this way (the subscript “n” denotes the normalization to the initial mass, M_i , of a CSP) is shown in Fig. 1 (left). For the purpose of its efficient implementation into the N-body code, we carry out a least-squares fit. The power-law fit, $\dot{M}_n(t) \propto t^{-y}$ suggests a very simple form since it gives $y = 1.04$, very close to unity. Rather than using 1.04, we fix $y = 1$, and perform a new least-squares fit with a hyperbola having a shift T_0 from the moment t_{birth} , at which a CSP was born, to avoid the unphysical singularity

Table 1. Fitted mass-loss rate parameters

τ [Gyr]	c_0	T_0 [Myr]
5	$5.55 \cdot 10^{-2}$	5.04
10	$5.47 \cdot 10^{-2}$	4.97
15	$5.41 \cdot 10^{-2}$	4.92
20	$5.35 \cdot 10^{-2}$	4.86

Table 2. Cumulative mass-loss of a CSP

Cumulative mass-loss at several chosen times (in Gyr) for the Scalo's IMF (1998) and Padua $Z = 0.02$ stellar models.

$R_{t=0.1}$	$R_{t=1}$	$R_{t=5}$	$R_{t=10}$	$R_{t=15}$	$R_{t=20}$
0.170	0.280	0.382	0.416	0.434	0.445

of the t^{-1} function at t_{birth} :

$$\dot{M}_n(t) \equiv \frac{\dot{M}(t)}{M_i} = \frac{c_0}{t - t_{\text{birth}} + T_0}. \quad (2)$$

We restrict the least-squares fits to combinations (c_0, T_0) giving the correct total gas return (cumulative mass-loss) R_τ over time τ (see Sect. 2.2. and Table 2), corresponding to the time interval between the birth of a given CSP and the envisaged end of an N-body simulation. Results of the fit for $\tau = 5, 10, 15$ and 20 Gyr are summarized in Table 1.

The fit for the simulation length of 20 Gyr is shown in Fig. 1 (left) by a dashed line. It is close at all times and over four orders of magnitude on the $\dot{M}_n(t)$ axis to the original dependence. It is also obvious, from Table 1, that the fits for different τ are very similar. We will take advantage of this when implementing the mass-loss into the N-body code: only one fit will be used for all the particles (see Sects. 3.4. and 3.5.).

2.2. Cumulative mass-loss of a coeval stellar population

While the time-dependence of mass-loss rate of a CSP is a vital input for our models, the cumulative mass-loss, i.e. the mass fraction lost by stars until time t after the birth of the CSP,

$$R_t = \int_0^t \dot{M}_n(t') dt', \quad (3)$$

gives a useful estimate of the importance of gas recycling on different time-scales.

Fig. 1 (right) shows, in the lower half of the plot, R_t of a CSP computed for the Scalo's (1998) IMF and the Padua $Z = 0.02$ stellar models. The curve in the upper half of the plot gives the fractional mass remaining in stars, i.e. $1 - R_t$. Table 2 gives R_t for $t = 0.1, 1, 5, 10, 15$ and 20 Gyr.

A discussion of mass-loss for other IMFs and stellar metallicities is beyond the scope of this paper. R_t for several other IMFs widely used in the litterature (Salpeter 1955; Miller & Scalo 1979; Kennicutt 1983) as well as for the Padua stellar models corresponding to $Z=0.0004, 0.004, 0.008, 0.02, 0.05$ is tabulated in Jungwiert (1998). Here we note only a few facts. For $Z = 0.02$, the highest gas return over the Hubble time (let's say 15 Gyr) is obtained for the Scalo's (1998) and Kennicutt's (1983) IMFs ($R_{15 \text{ Gyr}} = 0.43$ and 0.44, respectively), followed by the Miller & Scalo's (1979) IMF (0.41), while the Salpeter's (1955) IMF gives a markedly lower value (0.30). In all the cases, the returned mass fraction is considerable. As for the relative contributions of LMS, IMS and HMS to the total mass-loss, they are comparable, so that no category can be considered as significantly dominant. For example, the Scalo's (1998) IMF and $Z = 0.02$ stellar models lead to ratios LMS : IMS : HMS $\sim 1 : 1.25 : 1$ for the contributions to $R_{15 \text{ Gyr}}$. The stellar metallicity does not change the mass-loss of the whole CSP too much despite the fact that individual stars have their lifetimes and final masses influenced by Z quite noticeably (see Figs. 16 and 17b in Jungwiert 1998).

2.3. Galactic gas return rate

We define, for the purpose of simulations presented in Sect. 4, *gas return rate (GRR)* as the analog of star formation rate (*SFR*): GRR (units of $\text{M}_\odot \text{ yr}^{-1}$) is the rate at which stellar mass is converted into gaseous mass. In general, GRR depends on the whole history of star formation:

$$GRR(t) = \int_0^t SFR(t') \dot{M}_n(t - t') dt', \quad (4)$$

where $\dot{M}_n(t - t')$ is the (normalized) mass-loss rate, at time t , of a stellar population born at t' . Note that when GRR refers to a specified area, SFR in Eq. (4) does not refer to the same area: GRR at time t is not determined by the star formation history of this area but by the star formation history of stellar matter that is now present in this area but has, in general, various orbital histories.

3. N-body code with star formation and time-dependent stellar mass-loss

3.1. Gravitational interaction and equations of motion

We use the standard particle-mesh (PM) technique (Hockney 1970; Hohl 1971; for a review, see: Hockney & Eastwood 1981; Selwood 1987) to compute the gravitational potential on a Cartesian grid via Fast Fourier Transform (FFT). Forces at grid points are then evaluated by differencing the potential. Both the assignment of particle masses to grid points and the finding of forces between them are carried out by the bilinear “cloud-in-cell (CIC)” interpolation. The equations of motion are inte-

grated by means of the leap-frog algorithm (Hockney & Eastwood, 1981).

The gravitational softening that reduces interparticle forces at short distances (see Pfenniger & Friedli 1993) is that of a Plummer sphere. The choice of the softening length is done with regard to the criteria laid down by Romeo (1994, 1997) to optimize the stability and relaxation properties of N-body disks.

3.2. Particle species

There are four particle species in our code. Apart from relatively massive stellar particles (hereafter referred to as “standard stars”), typically representing millions of stars, and relatively massive gaseous particles (hereafter “clouds”) with characteristic masses of $10^5 - 10^6 M_{\odot}$, we introduce low-mass stellar and low-mass gaseous particles (hereafter nicknamed “starlets” and “cloudlets”) that mediate the exchange of matter – converted from gaseous to stellar phase and vice versa by star formation and stellar mass-loss – between the standard stars and clouds. The definition of mass boundaries between cloudlets and ordinary clouds and between starlets and ordinary stars, and thereby the mass ranges for cloudlets and starlets, are precised in Section 4.1. (item 13).

The standard clouds are meant to simulate the cold gas component. They are modelled as finite-size particles that undergo physical collisions in which they dissipate a fraction of kinetic energy. The relative velocity of two colliding clouds is reduced by factors β_r , β_t ; the former multiplies the velocity component along the line joining the two clouds (radial component), the latter perpendicular to it (tangential component) (for pioneering use of this “sticky-particles” technique in simulations of galaxies, see Schwarz 1981; among more recent applications and discussion on values of β_r , β_t , see e.g. Jungwiert & Palouš 1996).

Star formation is allowed to proceed in our cold gas component in the way described in Sect. 3.3. It results in the production of the above mentioned starlets. These in turn join the standard stellar component by merging with a standard star provided some is near by (typically 200 pc; to be precised below). On the other hand, standard stars lose continuously mass in the form of the cloudlets – as detailed in Sect. 3.4. – that join the cold gas component by merging with a standard cloud provided some is near by. The condition of particle “nearness” for star-starlet or cloud-cloudlet merging ensures that the mass exchange between the stellar and gaseous components is local.

In usual situations the existence of our starlets and cloudlets will be ephemeral since they will merge with a nearby standard particle immediately after they are born. This is technically equivalent to a direct exchange of a fraction of mass between a standard stellar and a standard gaseous particle. However, there are important and frequent astrophysical situations in which stars and cold gas are segregated spatially. For example, in some areas

cold gas can be depleted by intense star formation or swept away by gravity torques. There can also be regions of cold gas without any or with only small amounts of stars, for instance the whole galaxies in early evolutionary stages or, in the case of present-day galaxies, the area beyond the periphery of optical disks.

Our starlets/cloudlets enable to follow such situations. If a starlet/cloudlet is produced in an area (defined below) with no standard star/cloud, it leads an independent and possibly long-term existence until it meets the respective standard particle (meanwhile, the starlet is subject to mass-loss as standard stars and it produces cloudlets). The long-living starlets/cloudlets can also meet another starlet/cloudlet. Such events are treated by starlet-starlet and cloudlet-cloudlet mergings. In the course of time, a starlet/cloudlet grown by successive mergings of starlets/cloudlets might approach the mass typical of standard stars/clouds. If this occurs, the starlet/cloudlet is converted into a standard star/cloud. Conversely, a standard cloud is changed over to a cloudlet if its mass falls, due to the starlet production, below the value typical of standard clouds. In contrast, we do not consider a conversion of standard stars into starlets since the mass of a standard star remains of the same order during a simulation: it cannot decrease below the quantity $1 - R_{t_{\text{end}}}$ that is larger than ~ 0.55 for any simulation length t_{end} shorter than 20 Gyr (see Table 2).

In this respect, the cloudlets can be viewed as a very crude representation of the warm/hot galactic gas: they are products of star formation and do not participate in the star forming process unless they “cool” in areas of high gas density (either by merging with a standard cloud or with many other cloudlets).

In summary, the four particle species have the following properties. *Standard stars* produce cloudlets and can absorb starlets. *Starlets* can be absorbed by standard stars or merge with other starlets; they produce cloudlets; if their mass exceeds a given value (M_{ss} , $\sim 10^5 - 10^6 M_{\odot}$, see Sect. 4.1., item 13), they are converted into standard stars. *Standard clouds* undergo mutual, partly inelastic collisions; they produce starlets and can absorb cloudlets; if their mass falls below a given value (M_{cC} , $\sim 10^5 M_{\odot}$, Sect. 4.1., item 13), they are converted into cloudlets. *Cloudlets* can be absorbed by standard clouds or merge with other cloudlets; if their mass exceeds the above mentioned M_{cC} , they are converted into standard clouds.

All the particle productions, absorptions, mergings and collisions happen in the mass and momentum conserving manner.

Perhaps the most questionable interaction in our code is the merging of a starlet with a standard star or another starlet. The real stellar fluid cannot dissipate energy; nevertheless, if new stars are born with a low velocity dispersion (as expected from the kinematics of parent gas clouds), the velocity dispersion of the real stellar fluid as a whole can decrease. We merge the particles for computational reasons, so as to keep their number low (see below); we are unable to follow every new born stellar particle

independently. In this context, the merging of standard stars with starlets can be viewed as very crudely mimicking the rejuvenation of the stellar fluid by newly born stars and the related decrease of its velocity dispersion. The merging of one starlet with another can seem more problematic but this process is relatively rare in simulations we present. However, we admit that the merging of stellar particles could in general bias the evolution of the stellar orbital structure, especially if the merged particles had very different velocities. This problem certainly merits further investigation.

As indicated above, the interparticle interactions (collisions, mergings) require the ability to identify nearby particles. The same is true for the star formation process described in the subsequent subsection. To find nearby particles in a CPU-efficient way, we divide a galaxy into a 2D rectangular grid (hereafter ‘‘interaction grid’’; for its specifications see Sect. 4.1., items 11 and 6); four lists (standard stars list, starlets list, standard clouds list and cloudlets list) are associated with it: within each of them, the particles are continuously sorted in such a way that their indices are stored in the order of the increasing index of the grid boxes. This permits a fast identification of all the particles in a given box at every time step. Particles located in a given box are considered as ‘‘nearby’’ in the above used sense. It is true that two particles from distinct neighbouring boxes may be closer to each other than particles within a same box. However, our concern is basically to have at most one starlet and one cloudlet per box and to achieve this in a computationally simple manner. The fact of ignoring interactions behind the box boundary is dynamically unimportant since it happens on distances below the dynamical resolution of the code.

The star-starlet, starlet-starlet, cloud-cloudlet and cloudlet-cloudlet mergings permit to keep a low number of particles. If starlets/cloudlets were not merged, they would soon proliferate in an unacceptable number since at each time step at which the star formation and mass-loss procedures are applied, roughly N_{boxes} ($\sim 10^4 - 10^5$) starlets/cloudlets are created. The merging rule usually leads to mergings of nearly all starlets/cloudlets with standard stars/clouds within the time step in which these starlets/cloudlets were created (see Sect. 4.3.) except areas or evolutionary stages where or when there is not enough stars or cold gas.

3.3. Star formation scheme

We impose a generalization of the Schmidt law for star formation (Schmidt 1959; for a recent review, see Kennicutt 1998), i.e. the surface density of star formation rate, μ_{SFR} , is proportional to a power of the gas surface density: $\mu_{\text{SFR}} = A \mu_{\text{gas}}^\alpha$.

Kennicutt (1998) gives $\alpha = 1.4$ as the ‘‘best-fit’’ for the observationally determined Schmidt law relating the mean surface density of SFR to the mean surface density of cold (molecular + atomic) gas in both galactic disks

and circumnuclear regions of disk galaxies. In our model, we keep the freedom of choosing α as an input parameter (typically 1 or 2). The Schmidt law is applied with a time step Δt_{SF} (longer than the time step used to integrate the equations of motion; Sect. 4.1., item 12) separately in each of the boxes of the interaction grid.

Inside a given box, star formation proceeds as follows: 1) The standard clouds list is used to compute the cold gas surface density. 2) If this density is non-zero (i.e. there is at least one standard cloud), a starlet is created with the mass computed according to the Schmidt law. 3) The starlet mass is subtracted from the standard clouds in amounts proportional to their masses. 4) The position and velocity of the starlet are found in such a way that the total momentum of the standard clouds and of the starlet is conserved. 5) Standard stars, if any, are found using their list. If there are some, one of them is randomly chosen to merge with the starlet. If there is no standard star, the starlets list is searched through for present starlets, if any, that immigrated from neighbouring boxes. If the search is positive, all the starlets in the box merge into one. Otherwise the new starlet will temporarily lead an independent existence as described in the previous subsection.

3.4. Stellar mass-loss scheme

In Sect. 2 we have evaluated the normalized mass-loss rate, $\dot{M}_n(t)$, of a coeval stellar population. Here our goal is to implement the mass-loss into the N-body code.

As described in two previous subsections, new stellar mass forms, in our code, from gas as starlets that can merge with nearby standard stars or other starlets. Our typical stellar particle (either a standard one or a starlet) therefore does not represent a CSP but has a complex star formation history since it consists of mass of starlets born at various times in addition to the mass it was assigned in the beginning of the simulation.

The exact treatment of the mass-loss – for the code purposes discretized in time with a step Δt_{ML} (Sect. 4.1., item 12) – would then require to keep in memory, for each stellar particle, its star formation history, i.e. initial masses of starlets that were incorporated into it and the times at which these starlets were born. The mass lost by stellar particle J at time t_l due to incorporated starlets would read:

$$\begin{aligned} \Delta M_J(t_l) &= \int_{t_l - \Delta t_{\text{ML}}}^{t_l} \sum_{k < l} m_{*J}(t_k) \cdot \dot{M}_n(t' - t_k) dt' = \\ &= \sum_{k < l} m_{*J}(t_k) \cdot \Delta M_n(t_l - t_k), \end{aligned} \quad (5)$$

where $m_{*J}(t_k)$ is the mass with which a starlet, incorporated into J at $t < t_l$, was created at time t_k (the incorporation could have happened later than at t_k), and $\Delta M_n(t_l - t_k)$ is the fraction of mass lost over $t_l - \Delta t_{\text{ML}}$ by the stellar mass born at t_k . Computing this sum for every stellar particle ($N_{\text{stars+starlets}} \sim 10^5$) in each step ($N_{\text{steps}} \sim 1000$ if mass-loss is applied every $\Delta t_{\text{ML}} \sim 10$

Myr over the Hubble time) and keeping in memory the arrays of m_* and t_k would be computationally very expensive.

We therefore introduce a much simpler manner to evaluate the mass-loss of stellar particles getting benefit from the fact that $\dot{M}_n(t)$ was shown to be reasonably well fitted by a simple analytical function with only two parameters (Eq. 2). The trick consist in using the same functional form for all stellar particles disregarding their star formation histories, while individually adjusting the two parameters whenever a new starlet is incorporated.

It is thus necessary to define how to change the relevant parameters when two stellar particles of different ages and masses merge, and to check whether or not such a change plausibly represents the sum of their mass-loss rates. Formulated mathematically, we want to find, for a particle J formed at time t_J by merging of particles R and S , born at t_R and t_S , parameters C_J and T_J such that the mass-loss rate of J (hereafter called the *combined* mass-loss rate), expressed as

$$\dot{M}_J(t) = \frac{C_J}{t - t_J + T_J}, \quad (6)$$

would have similar time dependence and total gas return as if particles R and S were followed independently. Eq. (5) is then replaced by the corresponding integral of eq. (6):

$$\Delta M_J(t_l) = -C_J \ln(1 - \frac{\Delta t_{\text{ML}}}{t_l - t_J + T_J}) \quad (7)$$

Since there are two free parameters, C_J and T_J , we can impose two conditions on the combined mass-loss. After trying several possibilities (for a more detailed analysis, see Jungwiert (1998), pages 52–58) we require Eq. (7) to give the correct cumulative mass-loss at two time moments: at the end of the simulation, t_{end} , and at an intermediate time, t_{im} , between t_J and t_{end} ; the choice of $t_{\text{im}} = t_J + 0.2 \cdot (t_{\text{end}} - t_J)$ proved to give good results. These two conditions can be expressed as

$$\int_{t_J}^{t_x} \dot{M}_J(t) dt = \int_{t_J}^{t_x} \dot{M}_R(t) dt + \int_{t_J}^{t_x} \dot{M}_S(t) dt, \quad (8)$$

where t_x denotes either t_{end} or t_{im} .

A priori, it was not ensured that our combined mass-loss approximation well represented the real sum of particles' mass-losses. However, the tests presented in Sect. 3.6. verify the adequacy of our approach.

Knowing how to combine the mass-loss rates of individual particles when they merge, it remains to be said what values of C_J and T_J we assign to particles that do not form by merging, i.e. to starlets at the moment of their birth and to standard stars, if any, present in the beginning of the simulation. Such can be viewed as representing coeval stellar populations. Comparing eqs. (2) and (6), we see that T_J is simply T_0 and C_J is c_0 multiplied by the mass of a particle at the moment of its birth, $t_{\text{birth}} = t_J$. Values of c_0 and T_0 are chosen from Table 1 (as we have mentioned in Sect. 2.1., the fits presented in Table 1 are very close to each other; we will use that for $\tau = 10$ Gyr).

For the standard stars present in the beginning of the simulation, there is an additional issue consisting in defining their t_{birth} ; we postpone it to a special subsection below.

The last point is to explain what happens with masses ΔM_J lost by individual stellar particles at every time step Δt_{ML} . We use a strategy similar to that for star formation (Sect. 3.3.). The procedure runs through the interaction grid box by box: 1) All the standard stars and starlets are found using the respective lists and their ΔM_J (computed according to Eq. (7)) are summed up. 2) If the sum is non-zero (i.e. there is at least one stellar particle in the box), the mass is attributed to a new clouplet. 3) It is positioned to the center of mass of contributions ΔM_J coming from individual stellar particles and its velocity is computed in such a way that the total momentum of stellar particles in the box and of the clouplet itself is conserved. 4) The standard clouds, if any, are found using the clouds list. If there are some, one of them is randomly chosen to merge with the clouplet. If there is no standard cloud, the clouplets list is searched through for clouplets, if any, that immigrated from neighbouring boxes. If the search is positive, all the clouplets in the box merge into one. Otherwise the new clouplet will temporarily lead an independent existence.

3.5. Mass-loss of pre-existing stars

The purpose of this subsection is two-fold: first, to draw attention to the fact that when a simulation of a galaxy starts from a state in which a stellar component is already present, as is the case of numerous published works, it is natural and important to take into account its mass-loss; second, to define t_{birth} and C_J for standard stellar particles representing this component (hereafter “pre-existing stars” and “pre-existing stellar component”).

To know at what rate the pre-existing stellar component should lose mass during the simulation, an assumption must be made about the star formation history of the model galaxy. Here we restrict our attention to two extreme cases, a constant star formation rate over some epoch prior to the start of the simulation (defined by $t = 0$) and a starburst at some moment prior to the start of the simulation. To be more specific, we suppose a simulation of length $t_{\text{end}} = 10$ Gyr and calculate what gas mass, ΔM_{gas} , is released *during the simulation* (i.e. between $t = 0$ and t_{end}) by the pre-existing stellar component. Table 3 gives this mass (relative to the mass of the pre-existing stellar population at $t = 0$) for two constant *SFR* histories (lasting 5 and 10 years) and two starbursts (occurring 5 and 10 years prior to the start of the simulation):

The values of ΔM_{gas} range between 5 and 15% of the pre-existing stellar mass. This can represent a huge amount of gaseous matter in absolute terms. For example, starting a simulation with a stellar component of $4 \cdot 10^{10} M_{\odot}$ (as will be the case of our illustrative sim-

Table 3. Gas released by pre-existing stars

pre-simulation SF:	$\frac{\Delta M_{\text{gas}}(t_{\text{end}}=10 \text{ Gyr})}{M_{\text{stars}}(t=0)}$
const. <i>SFR</i> (-5 to 0 Gyr)	0.153
const. <i>SFR</i> (-10 to 0 Gyr)	0.115
starburst (-5 Gyr)	0.084
starburst (-10 Gyr)	0.050

ulation in Sect. 4) implies that the gas mass released from these stars between $t = 0$ and $t_{\text{end}} = 10$ Gyr would range between $2 \cdot 10^9 M_{\odot}$ and $6 \cdot 10^9 M_{\odot}$ which is typical of gas mass in disks of observed present-day spiral galaxies. The mass-loss of pre-existing stars is thus quite important and should not be neglected in simulations.

Technically, to be able to use Eq. (7), we need to assign to each of the pre-existing star (having mass M_0 at $t = 0$) a birth time, $t_{\text{birth}} = t_J$, and a birth mass, M_{birth} (the latter will give us C_J after multiplying by c_0). In the starburst case, all such particles have t_{birth} simply equal to the time moment of the starburst; in the case of a constant *SFR* history, we draw t_{birth} for each pre-existing particle randomly within the period of constant star formation epoch. Once we assign t_{birth} , M_{birth} is found by integrating Eq. (2) backwards in time (from $t = 0$ to $t_{\text{birth}} < 0$).

Pre-existing stars are thus supposed to have already lost mass $M_{\text{birth}} - M_0$ prior to the start of the simulation, however their mass-loss will continue also during the simulation.

3.6. Tests

Several tests of our mass-loss algorithm are described in Jungwiert (1998). Especially, it has been tested that the combined mass-loss (Sect. 3.4.) of a stellar particle built by merging (“composite particle” for the purpose of this subsection) of two or more stellar particles (“merged particles”) well approximates the sum of individual mass-losses for many mass and age ratios of merged particles and for many subsequent mergings. Five examples are shown in Figs. 2-4. In each row, the left pannel shows the mass-loss rate of a composite particle while the right pannel shows its mass and cumulative mass-loss (i.e. the gas mass it has released). Full lines represent quantities computed as if all the merged particles were followed independently (i.e. according to Eq. 5) while the dashed lines correspond to the combined mass-loss approximation (eqs. 6 - 8) used in our code. All the quantities are normalized to the sum of initial masses of merged particles.

Fig. 2 corresponds to a merging of two stellar particles of the same initial mass. The first one is born at $t = 0$, the second at $t = 5$ Gyr when the merging takes place. Fig. 3 shows the case of multiple mergings, equidistant in time, with all the merged particles having the same initial mass. The number of particles, N_{merge} , that have merged into the composite particle is 10 in the top row

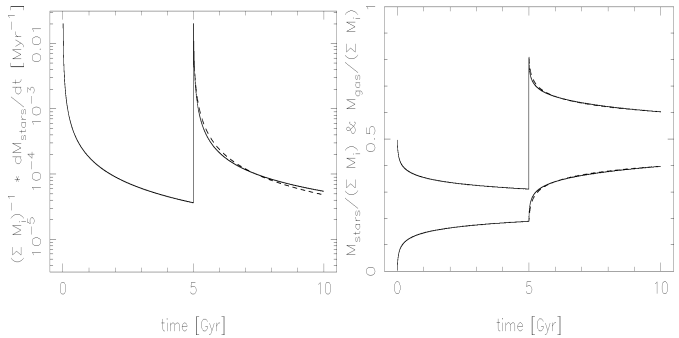


Fig. 2. Merging of two stellar particles born at $t = 0$ and 5 Gyr. **Left:** mass-loss rate of the composite particle; **right:** mass (M_{stars} , upper curve) and cumulative mass-loss (M_{gas} , lower curve) of the composite particle. Full lines in Figs. 2-4 correspond to exact sums of mass-losses of individual particles, dashed lines represent our combined mass-loss approximation.

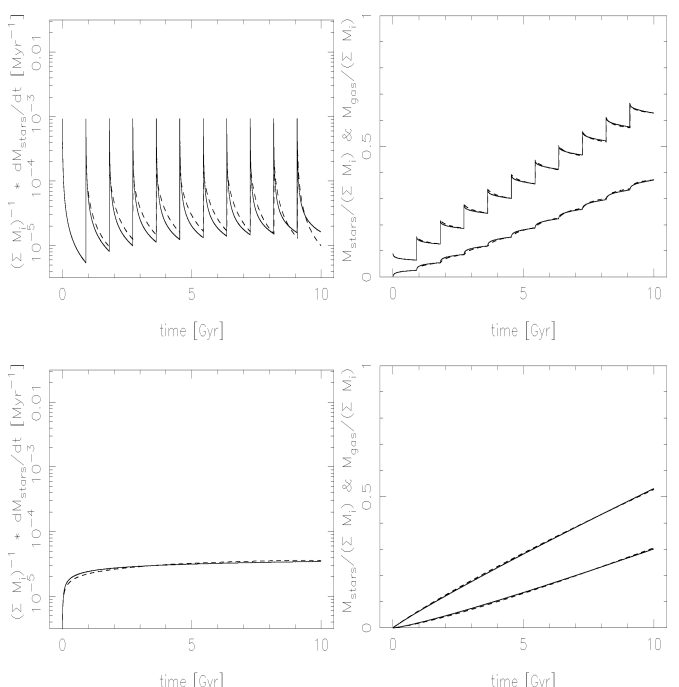


Fig. 3. Like Fig. 2 but for multiple mergings of particles having the same initial mass and born equidistantly in time. The particles merge at their birth. **Top:** $N_{\text{merge}} = 10$; **bottom:** $N_{\text{merge}} = 10000$.

and 10 000 in the bottom row. Fig. 4 also corresponds to $N_{\text{merge}} = 10$ (top row) and 10 000 (bottom row) but now the first particle is ten times, respectively ten thousand times more massive than the others it merges with. In all the examples presented in Figs. 2-4 the combined mass-loss approximation well represents the exact mass-loss. A few additional examples can be found in Jungwiert (1998, pages 52-58).

We have also carried out several runs of the N-body model in which the motion of particles was inhibited while the star formation and mass-loss schemes, producing cloudlets and starlets and combining them with standard clouds and stars, were operational. We have verified that

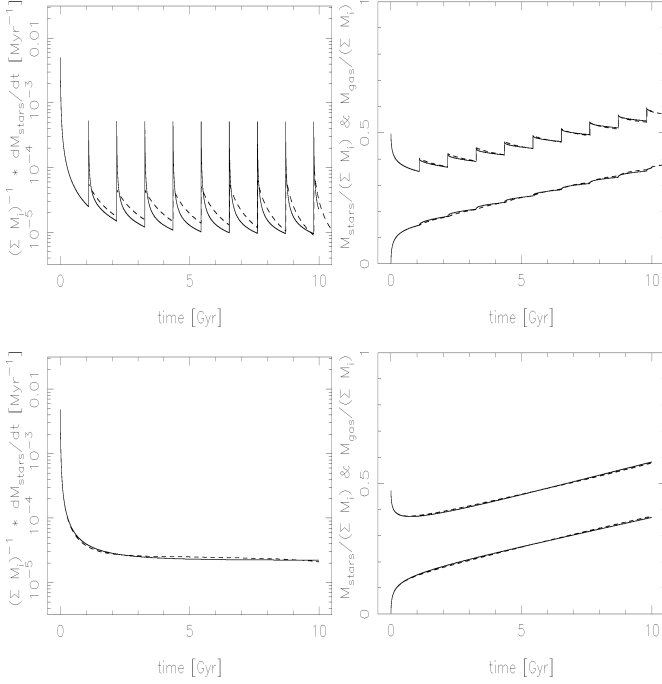


Fig. 4. Like Fig. 3 (i.e. multiple mergings of particles born equidistantly in time) but the initial mass of the first particle, $m_{i,1}$, is higher than initial masses, $m_{i,others}$, of other particles it merges with. **Top:** $N_{\text{merge}} = 10$, $m_{i,1} = 10 m_{i,others}$; **bottom:** $N_{\text{merge}} = 10000$, $m_{i,1} = 10000 m_{i,others}$.

these runs yield temporal evolutions for *SFR* and *GRR* close to numerical solutions of models not using any particles.

4. An example: a disk galaxy

As an illustrative application of our code, we present 4 simple 2-D models of a disk galaxy having no gas in the beginning of simulations. The first two models (denoted A and B) are rather artificial but useful reference cases: in model A stellar mass-loss is suppressed, the disk remains 100% stellar (classical purely stellar N-body model); in model B mass-loss from initial stellar particles produces gas but star formation is suppressed. The standard models (denoted C1 and C2) are those in which both star formation and stellar mass-loss operate: model C1 uses the linear Schmidt law ($\alpha = 1$), model C2 the quadratic one ($\alpha = 2$); stellar mass-loss is due both to initial and newly formed stellar particles. Table 4 summarizes basic attributes of the models. The simulation length is 10 Gyr for all of them.

4.1. Input data

For the sake of completeness and reproducibility, we enumerate, before describing the simulations, the code input parameters and specify their numerical values. The majority of them will be common to a larger set of models that will be published in a separate paper. Items 1-7 refer to parameters characteristic of collisionless N-body mod-

Table 4. Basic attributes of models

Model	star formation	mass-loss
A	no	no
B	no	yes
C1	yes, $\alpha = 1$	yes
C2	yes, $\alpha = 2$	yes

els, items 8-13 are specific to our gas dynamics and star formation/mass-loss schemes.

1) Initial stellar surface density (2D Toomre-Kuzmin disk: $M_{\text{disk}} = 4 \cdot 10^{10} M_{\odot}$, scale-length of 4 kpc, truncation radius of 16 kpc);

2) Initial number of stellar particles, $N_{\text{stars}} = 50000$; all of them have initially the same mass $M_0 = M_{\text{disk}}/N_{\text{stars}} = 8 \cdot 10^5 M_{\odot}$.

3) Initial velocity distribution. We fix the Toomre (1964) stability parameter $Q_{\text{stars}} = 1.5$ (constant in space), and then obtain velocities of particles by finding the time-independent axisymmetric solution of the Jeans equations; the ratio of azimuthal-to-radial velocity dispersions is computed using the epicyclic approximation (see e.g. Binney & Tremaine 1987);

4) Bulge and halo masses ($M_{\text{bulge}} = M_{\text{disk}}$, $M_{\text{halo}} = 5 \cdot 10^{11} M_{\odot}$) and scale-lengths (Plummer spheres of 1 and 25 kpc, respectively). The bulge is implemented essentially to partly stabilize the inner disk, the halo to keep the rotation curve flat in the outer disk. Both components (introduced by analytical formulae) are treated as unevolving;

5) Gravitational softening length (Sect. 3.1.), $s \approx 0.2$ kpc. It corresponds to the Romeo's (1994, 1997) "safe" softening computed for the center of our disk.

6) Number of divisions of the Cartesian grid used to compute the gravitational potential (Sect. 3.1.): $ND = 256$ (in each dimension). This number relates to the "active" grid (the computation proceeds on a grid doubled in each dimension as required by the FFT technique). The linear size of a grid cell, Δ_{grid} , is set equal to the softening length. The above choice of ND and s gives the linear size of the active grid, $D_{\text{grid}} = 50$ kpc (allowing for maximum disk radius of 25 kpc);

7) Time step for the integration of equations of motion, Δt . It is constant over the whole disk. Its value varies with time in such a way that it is 1/25 of the minimum orbital period. Initially $\Delta t = 0.6$ Myr. It decreases as the central mass concentration increases;

8) Parameters for cloud collisions (Sect. 3.2.): a) $\beta_t = 1.0$. This choice assures the conservation of angular momentum in a collision; b) $\beta_r = 0.6$. This choice is rather arbitrary. Varying β_r falls beyond the scope of this paper. We just note that a positive sign for β_r means, in our notation, that the direction of the cloud-to-cloud momentum in a collision is not reversed, unlike in most works implementing this collisional scheme. For more comments on values of β_r , see Jugwiert & Palouš (1996);

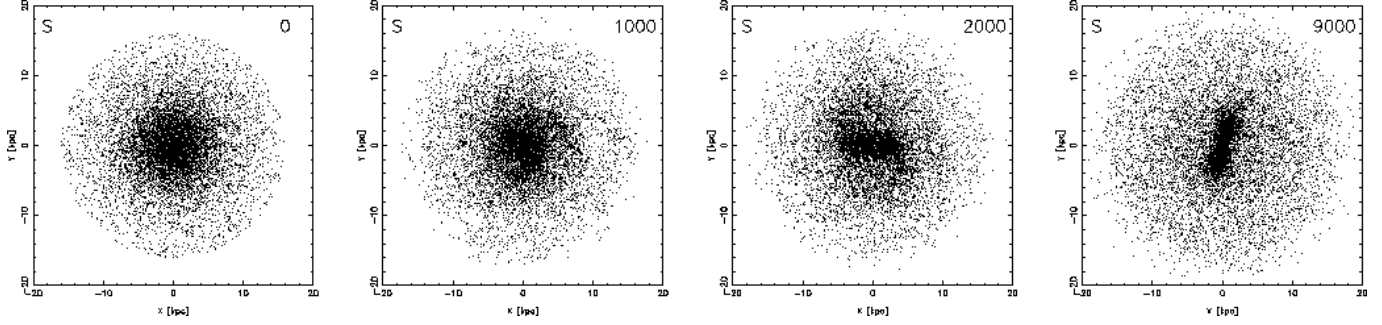


Fig. 5. Disk evolution in the purely stellar model A. In Figs. 5-7: numbers in the top right corner give time in Myr; only 20% of standard stellar particles, i.e. 10000, are shown for clearness.

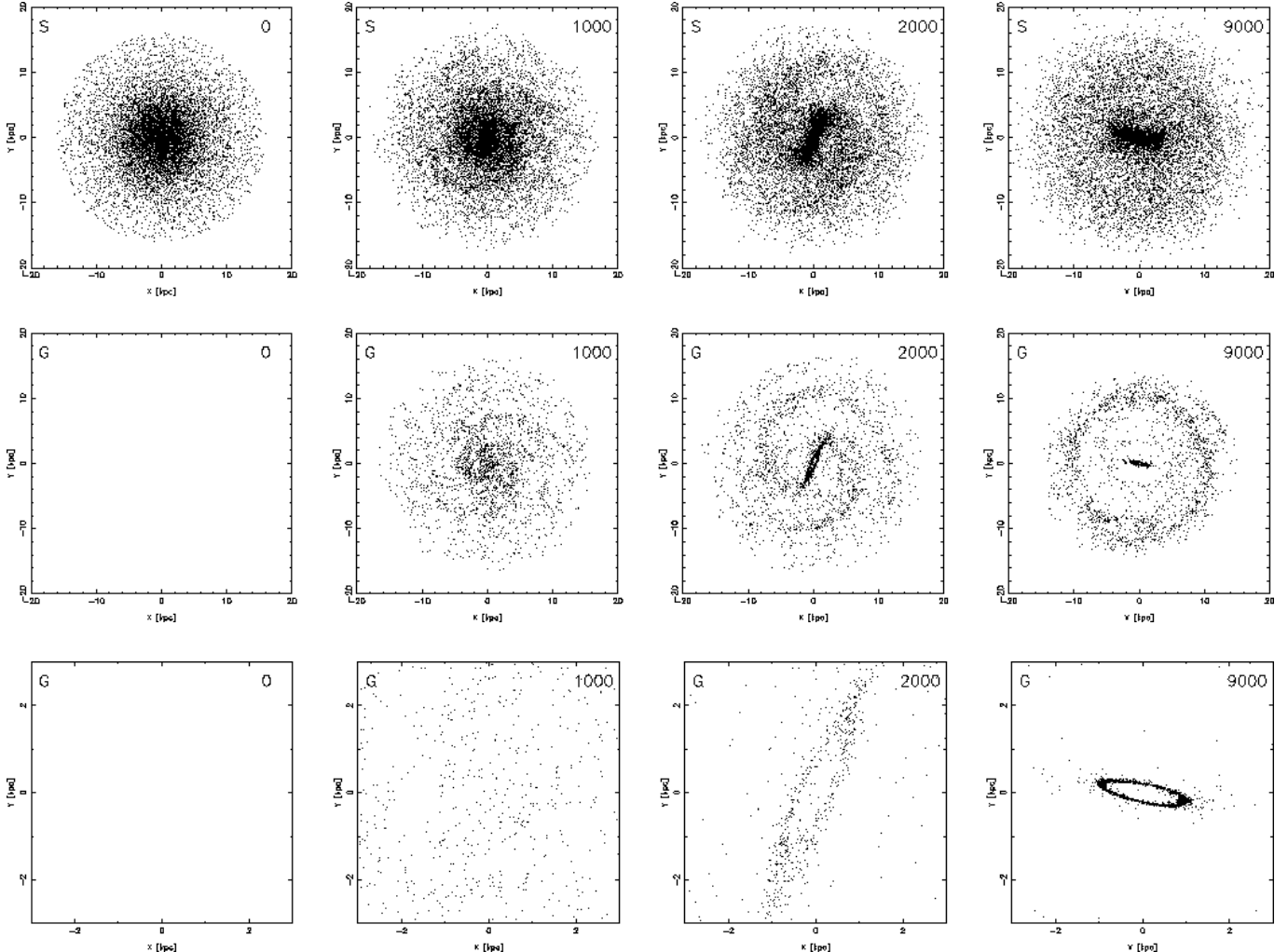


Fig. 6. Disk evolution in the standard model C1. **Top:** standard stars; **middle:** standard clouds; **bottom:** standard clouds – zoom to the central region.

9) Two parameters for the Schmidt star formation law (Sect. 3.3.): we choose $\alpha = 1$ or 2 and compute the proportionality constant A in such a way that the *SFR* value coincides with that of the Kennicutt's (1998) fit ($\alpha = 1.4$) at cold gas surface density of $5 \text{ M}_\odot \text{ pc}^{-2}$ (a value typical of present day-spiral galaxies);

10) Parameters related to the stellar mass-loss rate (Sects. 3.4. and 3.5): to assign t_{birth} to initial stellar particles, we use a simplifying arbitrary assumption that *SFR*

was constant over a period $T_{\text{SF}} = 5$ Gyr before the beginning of the simulation. c_0 and T_0 (that determine C_J and T_J of individual standard stars and starlets) are taken from Table 1 (for $\tau = t_{\text{end}} = 10$ Gyr);

11) The interaction grid (Sect. 3.2.) used for cloud collision, star formation and stellar mass-loss schemes has the same size and the same number of cells as the grid described in item 6;

12) Time steps Δt_{SF} (Sect. 3.3.) and Δt_{ML} (Sect. 3.4.) for applying star formation and mass-loss schemes. We fix $\Delta t_{SF} = \Delta t_{ML} = 6$ Myr (10 times the initial integration step Δt);

13) Masses M_{sS} and M_{cC} for star-starlet and cloud-cloudlet conversions (Sect. 3.2.). We fix $M_{sS} = (1 - R_{t=10\text{ Gyr}}) \cdot M_0 \sim 3.3 \cdot 10^5 M_\odot$, i.e. equal to the minimum mass to which the cumulative mass-loss R_t (Table 2) can drive a stellar particle with initial mass M_0 . As for M_{cC} , we set $10^5 M_\odot$; the overwhelming part of cold gas in galaxies seems to dwell in clouds with higher masses than this value.

4.2. Results

The disk evolution in the purely stellar model A and in the standard model C1 is shown in Figs. 5 and 6, respectively. Stellar disks (Fig. 5 and upper row of Fig. 6), initially axisymmetric, first develop transient spiral arms and then a long-lasting bar. Meanwhile, in model C1, stars release gas in the form of cloudlets. These gradually merge and in regions of high gas density form standard clouds (see Sect. 3.2.) that kinematically react to the non-axisymmetric potential and accumulate predominantly in a dense nuclear ring (Fig. 6, bottom row) and in an outer ring (Fig. 6, middle row), connected respectively to the inner and outer Lindblad resonances (ILR, OLR). A hint of another, weaker gaseous ring, surrounding the stellar bar and related to the 4/1 resonance, can also be seen.

For models B and C2 (Fig. 7, left and right pannels, respectively), we show only an advanced evolutionary stage ($t = 9$ Gyr) that can be compared with the last column snapshots of Figs. 5 and 6. In model B, one can note that the bar is shorter and rounder (than in all the other models), the outer ring is less regular (than in C1 and C2 models) while the nuclear ring has collapsed to a smaller size. All these differences are related to a huge gas release and associated bar weakening (for a review, see Combes 2001) that are discussed below. The disk structure and ring shapes in model C2 are rather similar to those of model C1, except that the standard (i.e. relatively massive) clouds in the nuclear ring are considerably depleted by a more intense star formation (resulting from a higher star formation efficiency at high gas densities).

As indicated under item 10 of Sect. 4.1., we have chosen the assumption of constant SFR over 5 Gyr preceding the start of the simulation. Given the initial disk stellar mass of $4 \cdot 10^{10} M_\odot$, Table 3 implies that the gas mass released by the pre-existing stars over the simulation is about $6 \cdot 10^9 M_\odot$. While our choice of the star formation history is arbitrary and favouring a rather huge mass-loss, Table 3 indicates that other choices would lead to a gas restitution by pre-existing stars in models B, C1 and C2 has important effects. First, it opens the way to star formation. Second, the presence of gas affects the radial transport of matter.

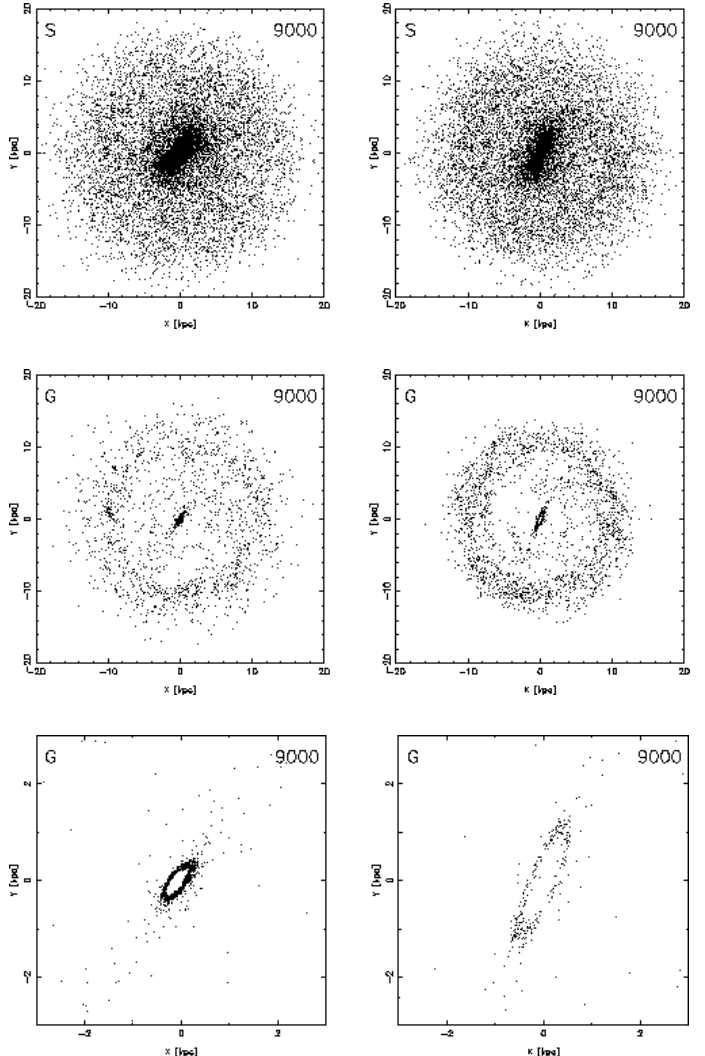


Fig. 7. Models B (left pannels) and C2 (right pannels) at $t = 9$ Gyr. **Top:** standard stars; **middle:** standard clouds; **bottom:** standard clouds – zoom to the central region.

gas restitution by pre-existing stars in models B, C1 and C2 has important effects. First, it opens the way to star formation. Second, the presence of gas affects the radial transport of matter.

As can be seen in Fig. 8, SFR is of the order of $1 M_\odot \text{ yr}^{-1}$ in the disk as a whole and, in the outer disk, it is pretty constant over the whole simulation, except early stages. The relative constancy of SFR is a result of the time-dependent recycling as was demonstrated by Jungwiert (1998) on a larger set of models, starting from either a two-component disk with $M_{\text{gas}}/M_{\text{stars}} = 0.1$ or from a purely gaseous disk. As for GRR , we note that, except early stages, contributions of the pre-existing stellar population and of stars formed during the simulation are comparable (the latter contribution corresponds to the difference between GRR curves for models C1 (or C2) and for the non-SF model B).

The transport of matter towards the center is quantified in Table 5 that shows the mean transfer rate of total

We show in Fig. 8, separately for the central disk region (here defined by $R < 2$ kpc) and for the outer disk ($R > 2$ kpc), temporal evolutions of SFR , GRR , total (i.e. stellar + gaseous mass) and gas mass fraction. The

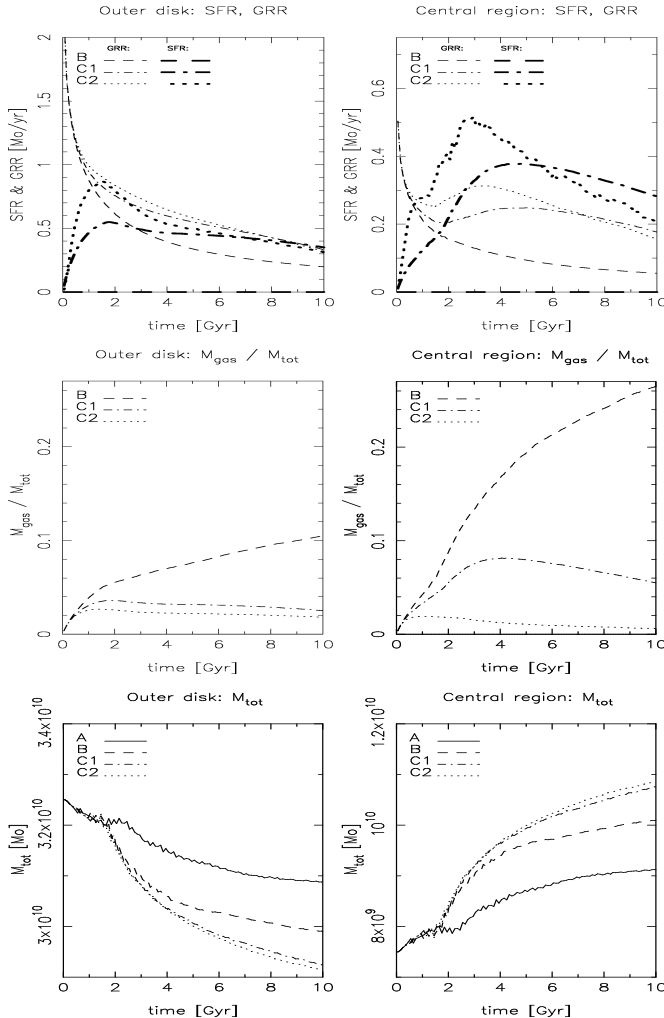


Fig. 8. Models A, B, C1, C2 – **left:** outer disk ($R > 2$ kpc), **right:** central region ($R < 2$ kpc); **top:** GRR (thin lines) and SFR (thick lines), **middle:** $M_{\text{gas}}/M_{\text{tot}}$, **bottom:** M_{tot} .

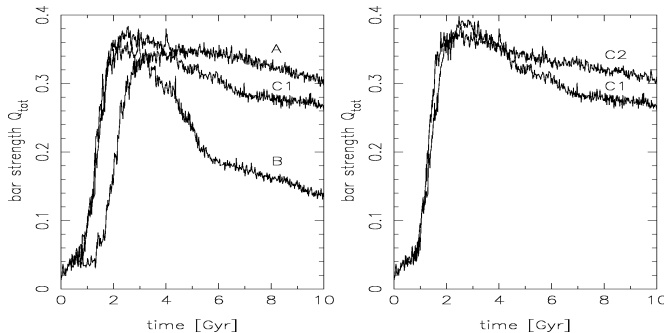


Fig. 9. Bar strength Q_{tot} – **left:** models A, B and C1; **right:** models C1 and C2.

(stellar + gaseous) mass into the central region ($R < 2$ kpc) and the relative strength of the bar, Q_{tot} (defined as the ratio of the maximum bar tangential force over azimuthally averaged radial force of the total force field; Combes & Sanders 1981; Buta & Block 2001) at 10 Gyr.

The radial transport is the least efficient in model A, as expected, since there is no gas. Model B is the most gas rich since mass-loss operates but star formation is

Table 5. Mean mass transfer rate (into $R < 2$ kpc) and bar strength

Model	$\langle \frac{dM_{\text{tot}}}{dt} \rangle_{\text{inflow}} [\text{M}_\odot \text{yr}^{-1}]$	$Q_{\text{tot}} (10 \text{ Gyr})$
A	0.17	0.30
B	0.27	0.14
C1	0.33	0.27
C2	0.34	0.30

Table 6. Gas mass fractions at 10 Gyr

Model	$\frac{M_{\text{gas}}(R < 2 \text{ kpc})}{M_{\text{tot}}(R < 2 \text{ kpc})}$	$\frac{M_{\text{gas}}(R < 2 \text{ kpc})}{M_{\text{gas}}(R < 20 \text{ kpc})}$
B	0.260	0.46
C1	0.055	0.45
C2	0.006	0.11

inhibited, however it is not the one with the largest inflow. The most efficient are models C1 and C2. This behaviour can be understood with the help of Fig. 9 that shows evolutions of the bar strength Q_{tot} . In model A, the bar instability appears after about 1.5 Gyr, the bar strength steeply grows until about 3 Gyr, then saturates at the value of ~ 0.33 and after 5 Gyr enters a phase of only slow secular weakening (at 10 Gyr, $Q_{\text{tot}} = 0.30$). The bar evolution in models B and C differs from model A in two respects. First, the bar appears earlier (instability starts before $t = 1$ Gyr and the saturation is reached at ~ 2 Gyr) since the gas production helps to destabilize the disk. Second, after saturation, there is more important weakening of the bar, especially pronounced in the gas rich model B (bar strength decreases from 0.35 to 0.14). This is connected to the known fact that a too important accumulation of matter near the center disturbs the bar orbital structure (Pfenniger & Norman 1990; Hasan & Norman 1990; Friedli & Benz 1993). The high gas fraction in the disk of model B thus first leads to a rapidly growing central concentration of gas (in the nuclear ring) which in turn disturbs the bar thus slowing down the future mass transfer (see Heller & Shlosman 1996).

The recycling models C1 and C2 thus provide, from the point of view of the efficiency in transferring matter inwards, the best combination of gas mass fraction and bar force, both quantities being interdependent.

Table 6 gives two gas mass fractions at the end of simulations: 1) ratio of gas-to-total mass inside the central region (here, “total” means gaseous + stellar but without the bulge contribution); 2) ratio of gas masses inside the central region and in the disk as a whole. In model B, about one quarter of the central region dynamical mass is in the form of gas. Note also that in models B and C1 roughly one half of the gas mass is located in the central region, i.e., more or less in the nuclear ring.

4.3. Computational efficiency and statistics of particle species

The presented algorithm for the continuous stellar mass-loss has a low computational cost. In the standard model C1, with 50 000 standard stars and active grid of size 256 x 256, the mass-loss and star formation related subroutines used about 12% and 3%, respectively, of the total CPU, its main part being spent on calculating the gravitational potential and advancing the particles. The simulations were carried out on a relatively slow one-processor PC Pentium II 366 MHz with one time step, Δt , taking on the average 0.9 sec.

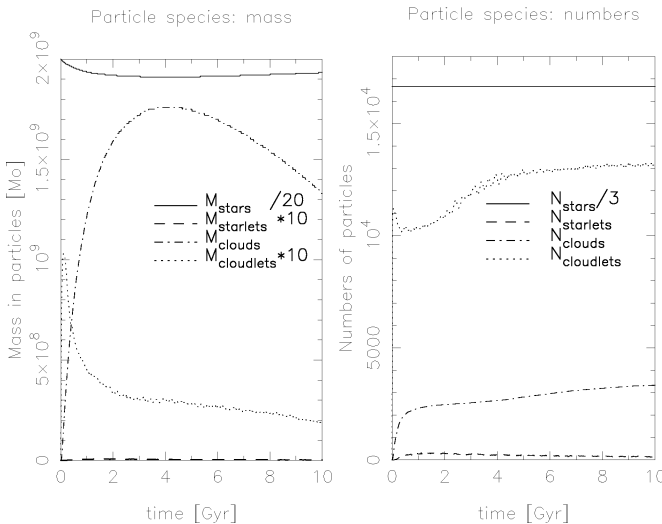


Fig. 10. Masses (left) and numbers (right) of different particle species (for convenience, the mass and number of standard stars are scaled down by factors of 20 and 3, respectively, while masses of starlets and cloudlets are scaled up by a factor of 10.

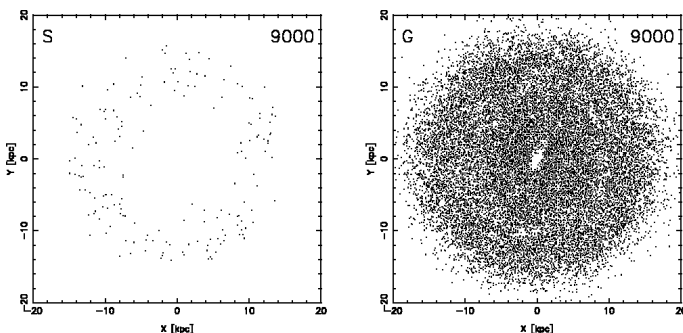


Fig. 11. Distribution of starlets (left) and cloudlets (right) in model C1.

Fig. 10 gives the statistics (masses and numbers) of the four particle species for the model C1. Fig. 11 shows spatial distributions of starlets and cloudlets.

The number of standard stars was constant. In principle, it cannot decrease since these particles have no way to disappear (except escapes that however did not occur) but it could rise due to starlets-star conversion after a starlet reaches the critical mass M_{ss} (Sects. 3.2. and 4.1., item 13); such conversions however did not happen. The mass

in standard stars slowly varies due to their mass-loss and absorption of starlets.

The number of standard clouds quickly (on a time-scale of ~ 500 Myr) grows (due to the initially copious stellar mass-loss) from 0 to ~ 2000 and then continues climbing only mildly (to 3300 at $t = 10$ Gyr). On the other hand, the overall mass in these particles reaches a maximum ($\sim 1.8 \cdot 10^9 M_\odot$) at about 4 Gyr and then declines (to $\sim 1.3 \cdot 10^9 M_\odot$ at $t = 10$ Gyr) due to intense star formation and decreasing mass-loss (cf. Fig. 8).

The number of starlets and the total mass in them are very low throughout the simulation (~ 200 and $10^6 M_\odot$) and negligible compared to standard stars. The starlets are thus almost virtual particles: despite a big number of them (of the order of 1000; one new starlet per box which hosts at least one standard cloud) is formed every time step Δt_{ML} (Sect. 4.1., item 12), the overwhelming majority is immediately incorporated to nearby standard stars. The only surviving starlets are located in outer parts of the galactic disk (Fig. 11, left) where the number of standard stars is low for the star-starlet mergings to work with the 100% efficiency.

The situation is somewhat different for cloudlets since their number is relatively high, between 10 000 and 13 000. However, their total mass is (except very early evolutionary stages) much lower (it is scaled up by a factor of 10 in Fig. 10 !) than the mass in standard clouds. Initially, the cloudlets happen to gather $\sim 10^8 M_\odot$ due to the mass-loss from initial standard stars, however they efficiently lose it in favour of the standard clouds (initially only by cloudlet-cloud conversions, later on also by cloud-cloudlet mergings). Cloudlets survive only in regions of low total gas density and most of the time harbour only a few $10^7 M_\odot$. Looking at Fig. 11 (right panel), one sees that the distribution of cloudlets is largely complementary to that of the standard clouds: cloudlets are depleted in high-gas-density regions, i.e. in the nuclear and outer gaseous rings. Note also that the cloudlet distribution extends beyond the outer edge of the standard cloud distribution (cf. Fig. 6).

Overall, our star-formation and mass-loss schemes with four particle species keep the total number of all particles ($\sim 65 000$) close to the initial value (50 000) and the various types of the particle species interactions do not put a heavy load on the CPU time.

5. Concluding remarks

We have presented a gas dynamical N-body model including star formation and time-dependent stellar mass-loss. The implementation of the latter feature is, both physically and technically, the most innovative element of our simulations and, as such, is the major result of this work. The related description should allow other people studying the galactic evolution by means of N-body simulations to transpose our mass-loss scheme into their codes.

Our code is obviously not free of shortcomings, for instance the ignorance of gas cooling and heating, inher-

ent to sticky-particles representation of gas (we however recall – see Sect. 3.2. – that our subdivision of gas particles into standard clouds and clouplets takes into account, on a very rudimentary level, at least some aspects of the gas cooling and of the gas transition from hot/warm to cold). Questions about the mergings of stellar particles were pointed out in Sect. 3.2. Other potentially important simplification is the neglection of the growth of metallicity on the stellar mass-loss. This will be remedied in the forthcoming research that will include the chemical enrichment.

We have carried out a simple 2D simulation of a disk galaxy starting with no gas. Its purpose was essentially illustrative. It should demonstrate the functionality and potential applicability of the developed code. Our intention was also to show, how the dynamics of classical purely stellar simulations could be altered if stellar mass-loss were taken into account.

It goes without saying that the choice of special initial conditions – on one hand, zero gas mass in the beginning of the simulation and, on the other hand, presumed constant star formation rate prior to the simulation – is not coherent. Nevertheless, such conditions can be approached in some astrophysical situations: during strong interactions between galaxies, gas is stripped from the outer parts of galactic disks (e.g. Moore et al. 1996) while that falling towards the center can be largely consumed by a nuclear starburst (e.g. Mihos & Hernquist 1996). A quietly star forming galaxy can thus be turned into a state without much gas. It can however be replenished by the stellar mass-loss as is the case of our simple model. Moreover, our results as for the rate of mass inflow, enhanced by the time-dependent recycling (relative to pure N-body calculations), seem not to qualitatively depend on our special initial conditions since they point in the same direction as the results we obtained for two-component disk models (Jungwiert 1998).

This work will be followed by a second paper dealing with the application of the presented code to disk galaxies with the emphasis on comparing the instantaneous recycling approximation with our time-dependent recycling, especially as to effects on star formation rate and radial transport of matter.

Acknowledgements. This research was carried out in the framework of the Czech-French project No. 9902 that is co-financed by the Academy of Sciences of the Czech Republic (AV ČR) and by the Centre National de la Recherche Scientifique (CNRS) and in the framework of the Key Project K1048102 of AV ČR. It was also partly supported by the grant No. A3003705 of the Grant Agency of AV ČR. We thank the anonymous referee for careful reading of the manuscript and for his suggestions.

References

Binney J., & Tremaine, S., 1987, *Galactic Dynamics*, Princeton University Press

Bressan, A., Fagotto, F., Bertelli, G., & Chiosi, C., 1993, *A&AS*, 100, 674

Buta, R., & Block, D. L., 2001, *ApJ* 550, 243

Combes, F., 2001, in: GH Advanced Lectures on the Starburst-AGN Connection, INAOE (ed. D. Kunth, R. Mujica), World Scientific, p. 223-277, astro-ph/0010570

Combes, F. & Sanders, R.H., 1981, *A&A* 96, 164

de Jager, C., Nieuwenhuijzen, H., & van der Hucht, K.A., 1988, *A&AS* 72, 259

Friedli, D., & Benz, W., 1993, *A&A* 268, 65

Hasan, H., & Norman, C., 1990, *ApJ* 361, 69

Heller, C.H., Shlosman, I., 1996, *ApJ* 471, 143

Hockney, R.W., 1970, *Methods Comput. Phys.* 9, 136 McGraw-Hill, New York

Hockney, R.W., & Eastwood, J.W., 1981 (reprinted 1989, 1992, 1994, 1999), *Computer Simulations Using Particles*, McGraw-Hill, New York

Hohl, F., 1971, *ApJ* 168, 343

Jog C.J., 1992, *ApJ* 390, 378

Jog C.J., 1996, *MNRAS* 278, 209

Jungwiert, B., 1998, *Bars, resonant rings, star formation and gas recycling in spiral galaxies*, PhD thesis, Paris Observatory (available upon request via ftp in postscript format)

Jungwiert, B., & Palouš, J., 1996, *A&A* 311, 397

Junqueira, S., & Combes, F., 1996, *A&A* 312, 703

Kennicutt, R.C., 1983, *ApJ*, 272, 54

Kennicutt, R.C., 1998, *ARA&A*, 36

Marigo, P., Bressan, A.G., & Chiosi, C., 1996, *A&A* 313, 545

Martinet, L., & Friedli, D., 1997, *A&A*, 323, 363

Mihos, J.C. & Hernquist, L., 1996, 641

Miller, G.E., & Scalo, J.M., 1979, *ApJ suppl.* 41, 513

Moore, B., Katz, N., & Lake, G., 1996, *Nature* 379, 613

Pfenniger, D., & Friedli, D., 1993, *A&A* 270, 561

Pfenniger, D., & Norman, C., 1990, *ApJ* 363, 391

Portinari, L., & Chiosi, C., 2000, *A&A* 355, 929

Romeo, A. B., 1994, *A&A* 286, 799

Romeo, A. B., 1997, *A&A* 324, 523

Salpeter, E.E., 1955, *ApJ*, 121, 161

Scalo, J., 1998, in: *The Stellar Initial Mass Function*, Proceedings of the 38th Herstmonceux Conference (ed. G. Gilmore, I. Parry & S. Ryan), astro-ph/9712317

Schmidt, M., 1959, *ApJ*, 129, 243

Schwarz, M.P., 1981, *ApJ* 247, 77

Selwood, J.A., 1987, *ARA&A* 25, 151

Tinsley, B.M., 1980, *Fund. Cosmic Phys.* 5, 287

Toomre, A., 1964, *ApJ* 139, 1217